International Journal of Mechanical Sciences 149 (2018) 452–458

Contents lists available at ScienceDirect

International Journal of Mechanical Sciences

journal homepage: www.elsevier.com/locate/ijmecsci

In situ electron microscopy tensile testing of constrained carbon nanofibers

Rajaprakash Ramachandramoorthy[a,b], Allison Beese[a,1], Horacio Espinosa[a,b,*]

[a] Department of Mechanical Engineering, Northwestern University, Evanston, IL 60208, USA
[b] Theoretical and Applied Mechanics Program, Northwestern University, Evanston, IL 60208, USA

ARTICLE INFO

Keywords:
Constrained carbon nanofibers
In situ SEM/TEM mechanical testing
Microelectromechanical systems (MEMS)
Electrospinning

ABSTRACT

Electrospun carbon nanofibers, produced from polyacrylonitrile (PAN) nanofiber precursors, with their superior mechanical properties, are promising candidates for manufacturing advanced polymer composites. Here, we report a series of tensile tests performed *in situ* under scanning electron microscope (SEM)/transmission electron microscope (TEM) observation, which show that the modulus and strength of electrospun carbon nanofibers can be enhanced through a simple mechanical constraint during the carbonization step in the electrospinning process. The constrained carbon nanofibers of diameter less than 150 nm were nanomanipulated inside the SEM onto a specialized microelectromechanical systems (MEMS) based testing platform and subsequently tested in uniaxial tension until failure. It was identified that both the strength and modulus of the constrained carbon nanofibers with sub-150 nm diameters are on average higher compared to their unconstrained counterparts by ~22% and ~31% respectively. Also, by evaluating the internal graphitic order of the constrained carbon nanofibers using TEM-based diffraction methods, we identified that the mechanical constraint during carbonization results in a better degree of orientation in the graphitic crystallites along the fiber axis. Finally, we use Weibull statistics for the deconvolution of the effects of diameter and the mechanical constraint on the tensile properties of carbon nanofibers. The Weibull analysis also showed that the comparatively superior strength of CCNFs is primarily due to better alignment of crystallites with the fiber axis.

1. Introduction

Carbon fibers are typically made from polyacrylonitrile (PAN) precursors using gel-spinning or electrospinning techniques. Using the gel-spinning technique, polymer fiber diameters in excess in ~5–10 μm can be produced, while fibers with smaller diameters of 10 nm to 1 μm can be obtained using the electrospinning technique [1]. These polymer fibers are then carbonized at high temperatures (800 °C–1200 °C) to obtain carbon fibers. Given the larger diameter and longer length of fibers produced using the gel-spinning technique, their mechanical properties can be characterized with relative ease, using miniaturized tensile testers, as has been reported extensively in the literature [2–4]. Such gel-spun carbon fibers have been reported to possess high strengths (>3 GPa) and moduli (>250 GPa) and have applications in fields ranging from automotive, aerospace and wind energy due to their extraordinary mechanical and electrical properties [3,5–7]. The mechanical properties of electrospun carbon fibers with even smaller diameters, on the nanometer scale, are expected to be better than larger gel-spun carbon fibers [5]. Also, from an application perspective, such small diameter carbon nanofibers (CNFs) are expected to improve the interactions with polymer matrices in advanced composites [8]. Yet, there are only a few reports in literature on the mechanical characterization of individual electrospun carbon nanofibers. This is because of the difficulties in manipulating these tiny fibers and the need for specialized microelectromechanical system (MEMS) testing platforms to conduct such testing [8–9]. Recently, such MEMS-based tensile testing platforms have been used in the literature for characterizing the mechanical properties of a variety of 1D nanostructures including nanowires [10–12], nanotubes [13] and nanofibers [9].

The exploration of methods to further improve the mechanical properties of carbon fibers has been a very active field of research over the past decade. Some of the techniques explored to improve their mechanical properties include irradiation using gamma rays [14], chemical treatments [15], and mechanical confinement [8–9]. Xiao et al. found that the carbon fiber strength and modulus can be increased by 16.1% and 17.4% respectively, by exposing the fibers to gamma radiation of 30 kGy [14]. Arshad et al. [8] and Beese et al. [9] tested electrospun CNFs of diameters ranging from 100 nm to 450 nm and found that both the strength and modulus of nanofibers increase significantly with de-

* Corresponding author at: Department of Mechanical Engineering, Northwestern University, Evanston, IL 60208, USA.
E-mail address: espinosa@northwestern.edu (H. Espinosa).
[1] Present address: Department of Materials Science and Engineering, Pennsylvania State University, 327, Steidle Building, University Park, PA 16802, USA.

https://doi.org/10.1016/j.ijmecsci.2017.09.028
Received 28 April 2017; Received in revised form 28 June 2017; Accepted 16 September 2017
Available online 21 September 2017
0020-7403/

creasing diameter, due to a confinement-based improvement in molecular alignment [16].

In this current work, we have explored an alternate way of improving the mechanical properties of CNFs, using mechanical constraint. Specifically, the polymer nanofibers synthesized using electrospinning were constrained mechanically during the carbonization process, which was conducted at 800 °C in a nitrogen rich atmosphere. The hypothesis was that the mechanical constraint of the fibers during carbonization would lead to a better alignment of the graphitic crystallites along the fiber axis, by preventing fast entropic shrinkage [17]. As such, by mechanically constraining the precursor fibers during carbonization at high temperatures, we prevented shrinkage and maintained a constant length in fibers that could lead to a loss of orientation in the crystallites. High temperature carbonization is known to increase the size of graphitic crystallites in the fibers, which is a requirement for producing high performance carbon fibers. It should be noted that the strength of carbon fibers increase with increasing carbonization temperature, as shown in literature [18]. In this study, we explore whether such superior properties can be achieved using mechanical constraint and lower temperature (800 °C), as lower temperatures are preferred from a processing and scaling-up standpoint. It is known that the failure in PAN based carbon fibers typically initiate from graphitic crystallites that are misoriented with respect to the fiber axis [16]. Thus, the effect of the mechanical constraint on aligning the graphitic crystallites with the fiber axis is investigated in this study, by comparing the structure–property relationships of carbon nanofibers of similar diameters which are fabricated at the same carbonization temperature of 800 °C, with and without mechanical constraint. Given that the mechanical properties of carbon fibers also improve with decreasing diameter, we have conducted mechanical metrology of constrained carbon nanofibers (CCNFs) with diameters below 150 nm, using a MEMS-based testing platform. We also collected selected area electron diffraction (SAED) patterns using a transmission electron microscope (TEM) to quantitatively measure the alignment of the graphitic crystallites with respect to the fiber axis and conducted Weibull analysis to further validate this claim. Thus, adding a simple mechanical constraint in the fabrication process can provide a new pathway for manufacturing high strength carbon fibers, especially if they are used in combination with the recently developed, sophisticated island-in-a-sea bi-component fiber spinning technique [19].

2. Materials and experimental methodology

The individual carbon nanofibers tested in this study were manufactured through an electrospinning process detailed elsewhere [20]. PAN nanofibers were produced using electrospinning at 12 kV with a 0.6 mL/h feed rate, a 20 ga needle, and a spinneret-collector distance of 20 cm. The nanofibers were subsequently stabilized under mechanical constraint in an oxygen atmosphere at 270 °C for 1 h. Stabilization at similar environmental conditions under mechanical constraint has been shown in previous works to promote the formation of condensed aromatic ladder-like structures [21–23]. These nanofibers were then carbonized, again under mechanical constraint, at 800 °C in nitrogen at a heating rate of 10 °C/min and dwell time of 1 h, to obtain CCNFs. The carbon nanofibers were constrained during carbonization to maintain a constant length which is analogous to applying a tensile force on the fibers [24]. It should be noted that the stabilization and carbonization was carried out on PAN nanofibrous mats under mechanical constraint and then individual CCNFs were extracted to conduct the mechanical testing.

CCNFs were tested using a MEMS based tensile testing device *in situ* under TEM and SEM observation. The MEMS device, as shown in Fig. 1, consists of V-shaped thermal actuator beams, shuttles across which nanofibers were mounted, and load sensing electrostatic fingers.

A 600 mesh copper TEM grid was cut in half, and then gently scraped over the electrospun and carbonized CCNFs mats to transfer some of the CCNFs onto the TEM half grid [25]. This grid was then placed inside a scanning electron microscope (SEM) (FEI NovaSEM 600) chamber along with a Klocke nanomanipulator, which controls a sharp tungsten tip with nanometer resolution, and the MEMS device. Using the tungsten tip attached to the nanomanipulator, the CCNFs were manipulated from the grid onto the shuttles of the MEMS device. The CCNFs were clamped onto the shuttles in the MEMS device using electron beam induced deposition (EBID) of a carbonaceous platinum spot weld.

Once a nanofiber was mounted across the shuttles of the MEMS device it could be tensile tested either within a TEM or an SEM. To perform *in situ* TEM tests, the MEMS device was first placed on a custom built TEM holder [26] and the holder was then loaded into a JEOL 2100 field emission TEM. A power supply was then used to apply an increasing voltage to the silicon beams of the thermal actuator. Subsequently, due to Joule heating the V-shaped silicon beams expand, resulting in an in-plane increase of gap between the two shuttles, across which the CCNF is mounted. Using digital image correlation, the displacement between the shuttles was obtained as a function of time during the test. Thus, during the test the displacement of the nanofiber is obtained from TEM images and immediately after the test the thermal actuator was calibrated by unloading using the same voltage steps to obtain the displacement of the thermal actuator as a function of applied voltage. In order to calculate the load applied on the nanofiber, the displacement of the load sensing shuttle was required. This load sensor displacement (d_{LS}) was calculated by subtracting the elongation of the nanofiber (d_{NF}) during the test from the calibrated thermal actuator displacement (d_{TA}) as shown in Eq. (1). The load applied on the nanowire was then calculated by multiplying the spring constant of the folded beams in the MEMS device by the displacement of the load sensor. The spring constant of the folded beams was calculated from beam theory using the beam geometry and the properties of the device material (silicon).

$$d_{LS} = d_{TA} - d_{NF} \tag{1}$$

While similar digital image correlation techniques can be used to ascertain the different displacements in the tests conducted in SEM, it will result in a higher error, due to the lower image resolution of the SEM compared to the TEM. In light of this, for the tests conducted inside SEM a differential capacitive sensing method is used to obtain the load [27]. To perform *in situ* SEM tensile testing of the mounted CCNF, a voltage was applied to the thermal actuator using a signal generator which provides continuous displacement at a strain rate of 5e−3 s^{-1}. The capacitive load sensor is suspended by a series of flexible folded beams functioning as a spring in series with the specimen, which can be thought of as another spring. Given that the load sensor experiences the same force as the specimen, the force applied on the specimen can be determined by measuring the displacement of the load sensor shuttle from equilibrium and multiplying it with the spring constant of the folded beams. The measurement of load sensor displacement is carried out electronically, by a series of capacitors (interdigitated fingers) formed between the moving shuttle and electrodes (or fingers) fixed to the substrate. Movement of the shuttle generates a capacitance change that can be detected electronically by a commercial integrated circuit and correlated to the displacement change. A detailed description of capacitive sensing can be found elsewhere [28]. Thus, contrary to the *in situ* TEM tests, during the *in situ* SEM tests the displacement of the load sensor was measured electronically through the changes in capacitance. However, the thermal actuator is calibrated in the same way as the *in situ* TEM experiments, using digital image correlation immediately after the test by unloading using the same voltage profile used for the nanofiber test. The displacement of the CCNF (d_{NF}) was obtained by subtracting the displacement of the thermal actuator (d_{TA}) obtained from calibration, and the displacement of the load sensor (d_{LS}), as shown in Eq. (1). The force and displacement were then converted to stress and strain, by dividing by the cross-sectional area of the nanofiber (fiber diameter measured from SEM images) and gauge length (~3.5 μm) respectively.

In order to determine the alignment of graphitic crystallites in the CCNFs, SAED studies were performed inside a TEM. The diffraction pat-

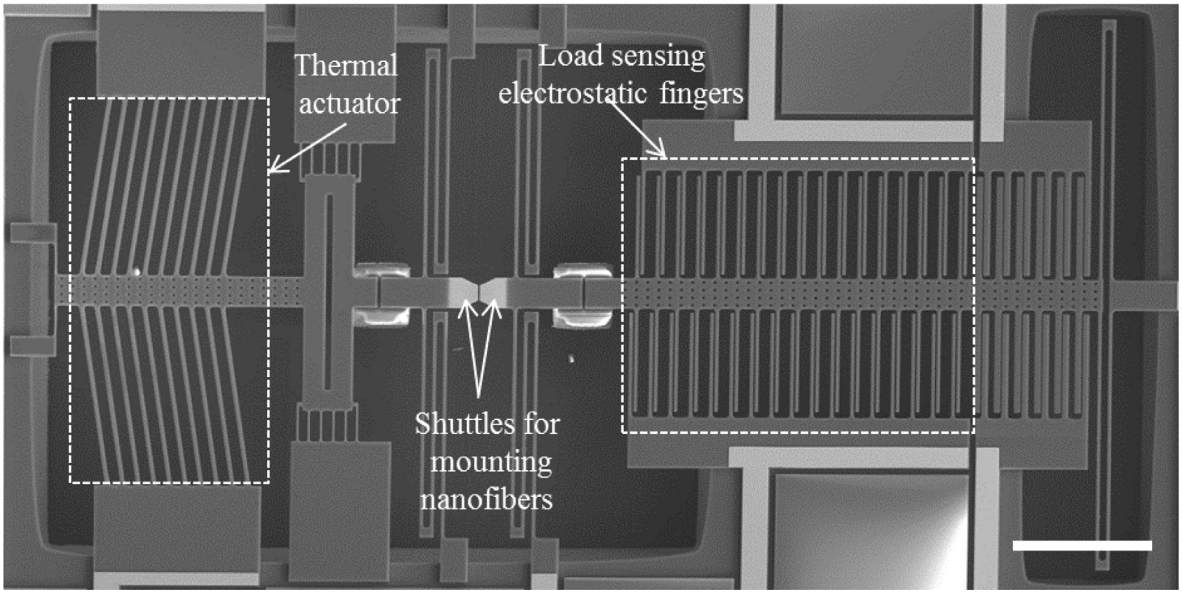

Fig. 1. MEMS based tensile testing device for testing *in situ* testing under SEM and TEM observation (Scale bar: 200 μm).

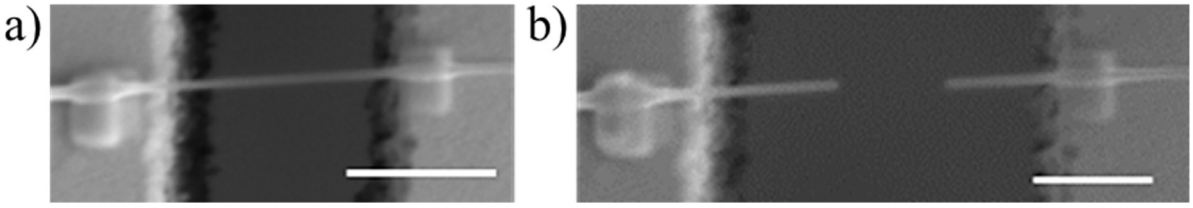

Fig. 2. Example of a CCNF (a) before and (b) after an *in situ* SEM tensile tests (Scale bars: 2 μm and 1.5 μm respectively).

terns were collected along the length of the CCNFs on a TEM grid with diameters of 40–185 nm. It should be noted that the mechanically tested CCNFs were a subset of these fiber diameters. The diffraction patterns of the (002) graphitic planes were studied to quantify the degree of graphitic crystallite alignment with the fiber axis in the CCNFs and the corresponding structure–mechanical property relationships were identified.

3. Results and discussion

In situ testing of fibers under TEM has unique advantages [29] such as the precise measurement of the diameter of the sample along the entire gauge length and the quantification of graphitic crystallite alignment within fibers [9]. But unfortunately, during the transfer of the MEMS device, with a nanofiber mounted, from the SEM to TEM the nanofibers can fail prematurely due to electrostatic discharge (ESD). As such, the success rate of sample survival is low, owing to the sensitivity of the MEMS devices to ESD. Thus, in this study only two samples were tested inside the TEM, while the rest of the CCNFs and unconstrained CNFs (similar to the fibers tested by Beese et al. [9]) were tested in SEM to prevent handling of the MEMS device after mounting, thereby increasing sample survival rate. In this study only sub-150 nm diameter fibers were tested and Fig. 2(a and b) shows a representative image of a CCNF before and after the tensile test respectively. Also, as seen from Fig. 2(a and b), nanomanipulation has resulted in a small error, as the CCNF has been mounted at a small angle with respect to the tensile axis. As such the forces calculated from the analysis of the tests have been adjusted to account for such misalignments, by taking the appropriate component. It should be noted that the EBID platinum spot welds used to clamp the CCNF to the shuttles can lead to a thin layer of amorphous carbon to be deposited within the gauge region of the nanofiber and additionally the SEM/TEM imaging of the CCNF can also lead to electron beam induced carbon deposition. However, following the calculations done by Filleter et al. [30], we find that the error in modulus due to this amorphous carbon layer will be less than 5% of the measured nanofiber properties.

Previously Beese et al. performed tensile tests on unconstrained CNFs using similar MEMS devices [9]. To compare the enhancement in mechanical properties due to the mechanical constraint during fabrication of the CCNFs, the results of the current study are plotted against the results with unconstrained fibers from the current and previous studies, [8–9] as shown in Fig. 3(a and b), where the modulus and strength values are plotted against the fiber diameters, respectively. The modulus and tensile strength values of the CCNFs on an average are indeed higher than the values obtained for the unconstrained CNFs tested and the mechanical properties increase with decreasing diameter. Also, both the tensile strength and modulus increase with decreasing diameter and an exponential fit has been provided in Fig. 3(a and b) as a guide for the reader. We hypothesize the reason for such higher strength and modulus values with decreasing diameter is because of the decreasing volume fraction that translates to lower initial defects in the fiber [9].

The carbonized PAN nanofibers typically have multiple graphitic crystallites in their volume. It is known that when these fibers are subjected to a tensile stress, the failure typically starts from the misoriented crystallites (see Fig. 4c)), as they are weakest in shear on the basal planes [16]. We hypothesized that the mechanical constraint during carbonization would lead to a better alignment of graphitic crystallites within the fibers, and therefore higher strength and stiffness.

In order to determine if the graphitic crystallites were indeed better oriented along the fiber axis in the CCNFs compared to the unconstrained CNFs, SAED studies were conducted on a TEM grid with CC-

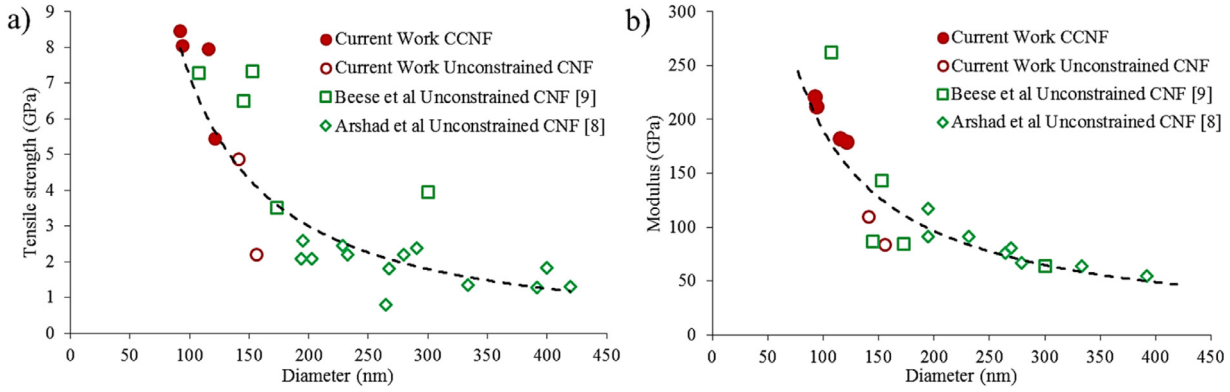

Fig. 3. (a and b) Tensile strength and modulus of CCNFs *versus* fiber diameter, compared with unconstrained CNFs from literature [8–9].

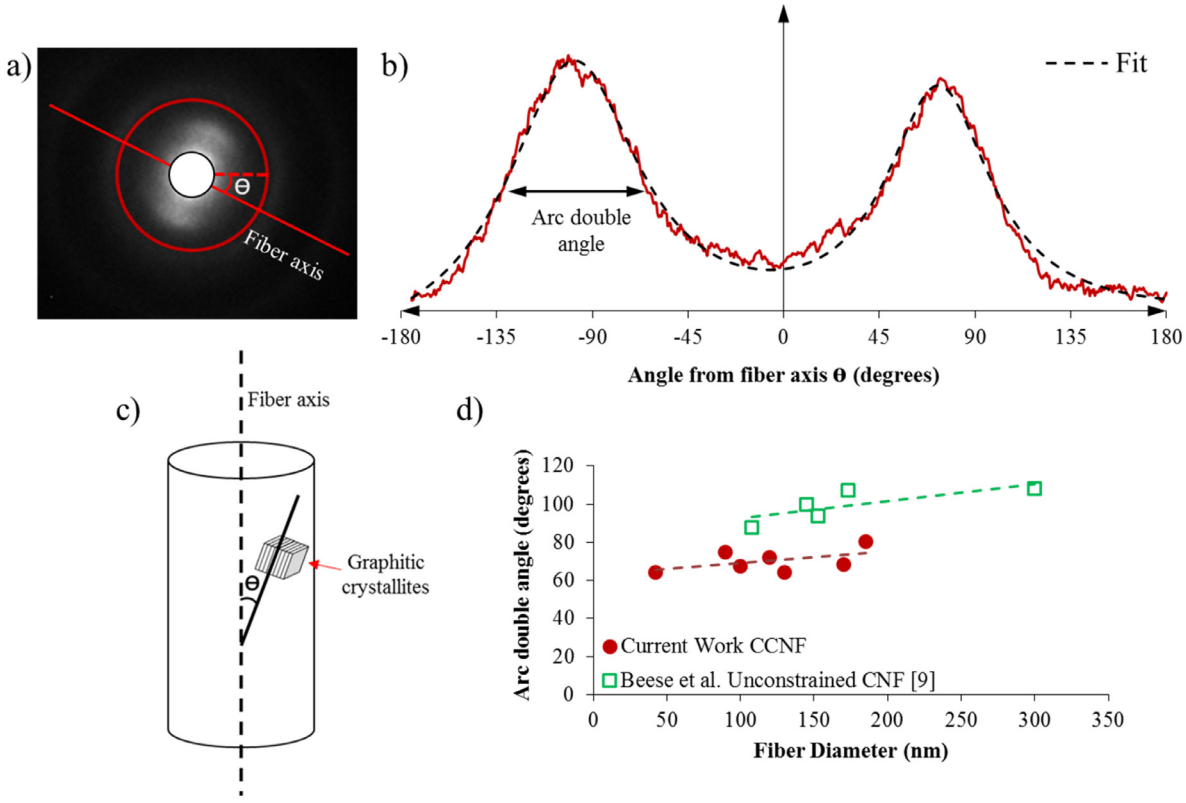

Fig. 4. (a) SAED pattern of a CCNF; (b) Analysis of the SAED image provides the intensities as a function of angle from the fiber axis; (c) Schematic showing the graphitic crystallites and their misorientation with the fiber axis; (d) Arc double angle of CCNFs compared to unconstrained CNFs [9] as a function of fiber diameter.

NFs in a JEOL 2100 TEM. SAED patterns, as representatively shown in Fig. 4a), for CCNFs with diameter varying from 40 to 185 nm were obtained and the full width half maximum (FWHM) of the integrated intensities (calculated as a function of angle from the fiber axis using QPCED2 software) of the (002) arc were obtained for all the inspected fibers, as shown in Fig. 4b). The FWHM was calculated for the two peaks in each SAED pattern and several SAED data points along the same fiber were obtained. The average of all these values was taken as the FWHM or the arc double angle for each fiber. A higher value of the arc double angle corresponds to a larger misorientation of graphitic crystallites with respect to the fiber axis, while a smaller value point toward increased alignment of these crystallites within the fiber axis [9]. As seen from Fig. 4d the CCNFs with a lower arc double angle have a better alignment of graphitic crystallites to the fiber axis compared to the unconstrained CNFs and as expected the alignment also improves with decreasing diameter in both the constrained and unconstrained fibers due to confinement effects.

In order to explore the structure–property relationships of the CCNFs and to compare them with these relationships obtained for the unconstrained fibers [9], the strength and modulus was plotted with respect to their arc double angles as shown in Fig. 5(a and b). It should be noted that for the fibers that were tested in the SEM, the arc double angle values corresponding to their fiber diameter were interpolated based on the fit from Fig. 4(d).

As seen clearly from Fig. 5(a and b), as the arc double angle decreases, and therefore, the orientation of the graphitic crystallites increase, the strength and modulus of the fiber increases in both the CCNF and unconstrained CNF. In addition, they show that the CCNFs, which

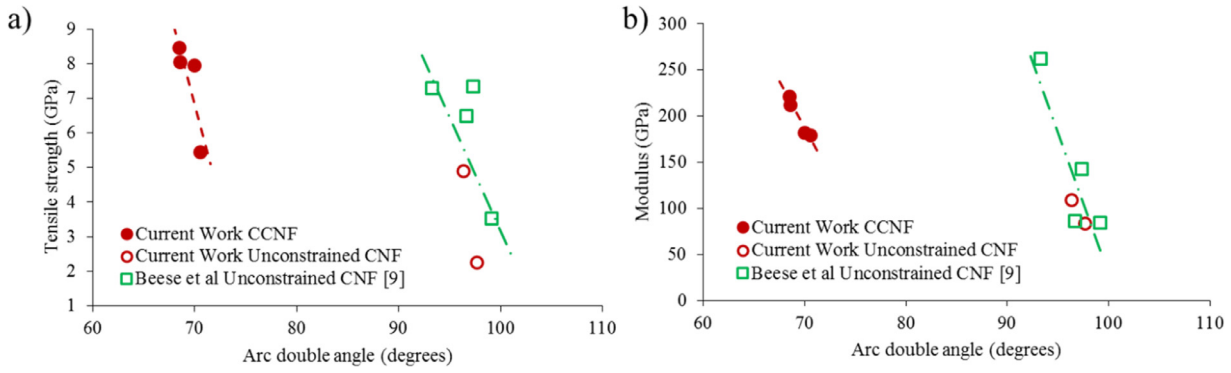

Fig. 5. (a and b) Structure–property relationships: Strength and modulus plotted with respect to their corresponding average arc double angle for CCNFs and unconstrained CNFs [9] (trends indicated in dashed lines).

Table 1
Experimental failure stress and calculated failure probability of CCNFs.

CCNF sample rank	Diameter (nm)	Failure stress (GPa)	Failure probability (P_f)
1	125	5.44	0.2
2	115.8	7.94	0.4
3	94.1	8.03	0.6
4	92.42	8.45	0.8

have increased orientation of the graphitic basal planes with the fiber axis compared to the unconstrained CNFs, have comparatively superior mechanical properties. In order to understand the reliability of CCNFs over unconstrained CNFs and to deconvolute the effects of diameter and mechanical constraint on their improved mechanical properties, we used Weibull statistics based on the Eq. (2) below [31–32]

$$P_f(V) = 1 - \exp\left[-\frac{V}{V_o}\left(\frac{\sigma - \sigma_o}{\sigma_o}\right)^m\right] \quad (2)$$

where σ is the failure stress, σ_o is the stress parameter at which 63% of the samples fail, m is the Weibull modulus, σ_u is the threshold stress that can be taken as zero for brittle materials [33], V is the volume of the fiber tested and V_o is reference volume that is taken as the smallest diameter fiber tested in this study. The fibers were first ranked in ascending order to their failure stress and then a failure probability of $n/(N+1)$, where n is the rank of the specimen and N is the total sample size, assigned to the fibers, as summarized in Table 1.

Subsequently, the Weibull stress parameter σ_o was identified as the 63% failure probability for both constrained and the unconstrained fibers. The CCNFs have higher fracture strength of 8.03 GPa compared to the 2.41 GPa of unconstrained CNFs for a failure probability 63%. Subsequently, the Weibull modulus was then identified for CCNFs and unconstrained CNFs using Eq. (2), by calculating the slope of the Weibull probability ($\ln(-\ln(1-P_f))-\ln(V/Vo)$) *versus* $\ln(\sigma)$ plot, as shown in Fig. 6. The CCNFs have a higher m of 4.76 compared to the 2.66 of unconstrained fibers, which shows that the constrained fibers are more reliable compared to the unconstrained fibers [32]. Given that the Weibull modulus is obtained after normalizing for the sample volume for both fiber types, the higher m value shows that the superior strength of CCNFs over unconstrained CNFs is definitely a structural effect, owing the improvement in the alignment of graphitic crystallites with the fiber axis. It should be noted, however, that due to the complexities involved in conducting nanofiber testing, the Weibull modulus has been calculated with limited data points and is potentially prone to errors. To confirm unambiguously the reliability of CCNFs, further testing is needed to obtain a larger sample size.

In summary, two features may lead to the increased strength with decreasing nanofiber diameter: the decreasing volume that translates to decreased room in the samples for initial defects, and thus, a decreased probability of failure, especially in brittle materials [34], and the mechanical constraint during carbonization that improves graphitic alignment with the fiber axis, resulting in stronger fibers. Also, given that the fibers tested in this study have several envisioned applications in composites and armor, Fig. 7 provides a comparison between the mechanical properties of these fibers and commercially available fibers reported in literature. As seen from Fig. 7, the CCNFs possess higher strength than any other PAN based fiber from literature. This high strength, as mentioned above, can be attributed to the nanoscale diameter and the better alignment of the graphitic crystallites with the fiber axis due to the constraint during fabrication. Also, it can be seen from Fig. 7 that Leon et al. observed a high strength in carbon fibers of diameter greater than 3 μm by applying progressively increasing cyclic tensile loads during fiber manufacture [35]. Thus, one possible future way to improve the mechanical properties of CNFs is to expose them to active tensile loading cycles during manufacture, rather than just keeping them constrained, as with CCNFs tested in this study.

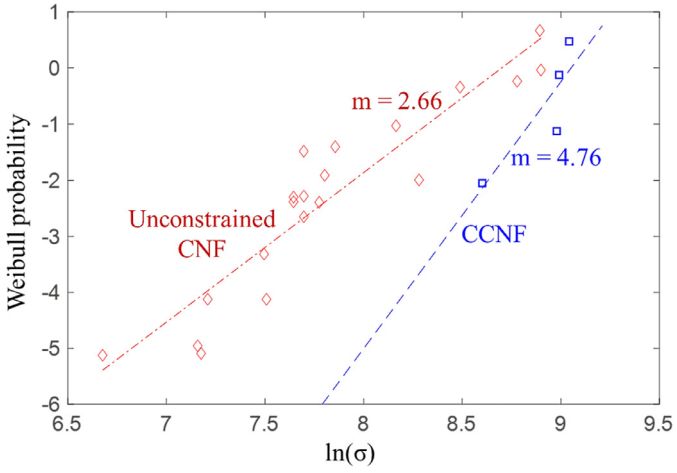

Fig. 6. Weibull exponent m for CCNF and unconstrained CNF.

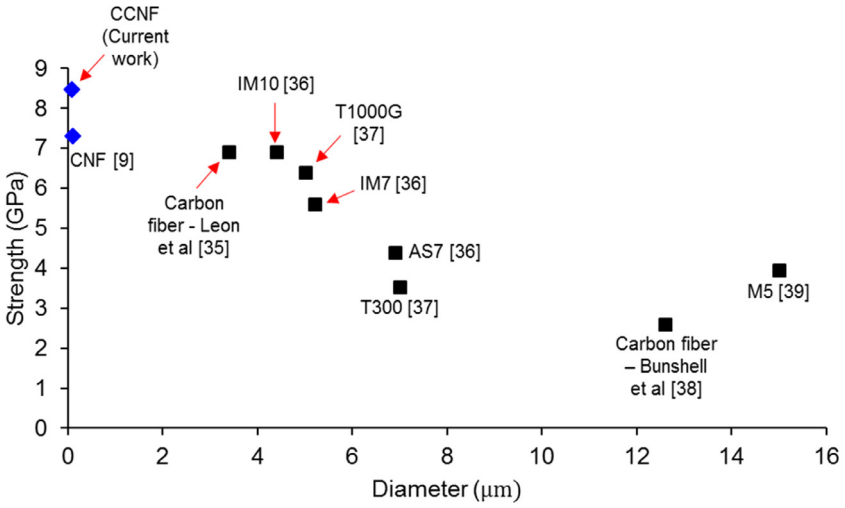

Fig. 7. Mechanical property comparison between CCNFs, CNFs [9] and commercial fibers [35–39].

4. Conclusions

In situ electron microscopy based structural and mechanical characterization of CCNFs was carried out to understand the effects of mechanical constraint during carbonization. We performed mechanical tests on a selected subset of CCNFs with sub-150 nm diameters using a customized MEMS based testing platforms and found that the modulus and strength increased with decreasing fiber diameter. We then compared the mechanical properties CCNF results with the unconstrained CNFs tested by Beese et al. [9] and Arshad et al., [8] and the CCNFs were found to be mechanically superior to the unconstrained fibers. As a method to identify and compare the structure–property relationships of the CCNFs and unconstrained CNFs, SAED studies were conducted. The results showed that the constrained fibers have better alignment of the graphitic crystallites with the fiber axis than the unconstrained counterparts. The structure–mechanical property relationships show similar trends for decreasing diameter in both constrained and unconstrained cases, as reduced initial defect density in the samples lead to an improved strength and modulus in the fibers. However, when CCNFs of a similar diameter are compared with unconstrained CNFs, CCNFs exhibit better structural alignment and mechanical properties. Thus, constraining the carbon nanofibers of sub-150 nm diameter before carbonization will result in an increasing degree of graphitic crystallite alignment with the fiber axis. This results in a mechanically superior and more reliable CNF, as ascertained from the Weibull modulus, compared to unconstrained CNFs, for a marginal increase in effort during nanofiber manufacture.

Acknowledgements

H.D. Espinosa gratefully acknowledges support from NSF through award No. DMR-1408901. We thank Prof. Y. Dzenis for providing the carbon fibers tested in this study. We also thank Dr. Shuyou Li for help with TEM imaging. This work made use of the EPIC, Keck-II, and/or SPID facility(ies) of Northwestern University's NUANCE Center, which has received support from the Soft and Hybrid Nanotechnology Experimental (SHyNE) Resource (NSF ECCS-1542205), the MRSEC program(NSF DMR-1121262) at the Materials Research Center, the International Institute for Nanotechnology (IIN), the Keck Foundation, and the State of Illinois, through the IIN.

References

[1] Fennessey SF, Farris RJ. Fabrication of aligned and molecularly oriented electrospun polyacrylonitrile nanofibers and the mechanical behavior of their twisted yarns. Polymer 2004;45(12):4217–25.
[2] Şahin K, Fasanella NA, Chasiotis I, Lyons KM, Newcomb BA, Kamath MG, et al. High strength micron size carbon fibers from polyacrylonitrile–carbon nanotube precursors. Carbon 2014;77:442–53.
[3] Chae HG, Newcomb BA, Gulgunje PV, Liu Y, Gupta KK, Kamath MG, et al. High strength and high modulus carbon fibers. Carbon 2015;93:81–7.
[4] Newcomb BA, Gulgunje PV, Gupta K, Kamath MG, Liu Y, Giannuzzi LA, et al. Processing, structure, and properties of gel spun pan and PAN/CNT fibers and gel spun pan based carbon fibers. Polym Eng Sci 2015;55(11):2603–14.
[5] Chae HG, Choi YH, Minus ML, Kumar S. Carbon nanotube reinforced small diameter polyacrylonitrile based carbon fiber. Compos Sci Technol 2009;69(3):406–13.
[6] Edie D. The effect of processing on the structure and properties of carbon fibers. Carbon 1998;36(4):345–62.
[7] Behabtu N, Young CC, Tsentalovich DE, Kleinerman O, Wang X, Ma AW, et al. Strong, light, multifunctional fibers of carbon nanotubes with ultrahigh conductivity. Science 2013;339(6116):182–6.
[8] Arshad SN, Naraghi M, Chasiotis I. Strong carbon nanofibers from electrospun polyacrylonitrile. Carbon 2011;49(5):1710–19.
[9] Beese AM, Papkov D, Li S, Dzenis Y, Espinosa HD. *In situ* transmission electron microscope tensile testing reveals structure–property relationships in carbon nanofibers. Carbon 2013;60:246–53.
[10] Ramachandramoorthy R, Wang Y, Aghaei A, Richter G, Cai W, Espinosa HD. Reliability of single crystal silver nanowire-based systems: stress assisted instabilities. ACS Nano 2017.
[11] Chen LY, He M-r, Shin J, Richter G, Gianola DS. Measuring surface dislocation nucleation in defect-scarce nanostructures. Nat Mater 2015;14(7):707–13.
[12] Ramachandramoorthy R, Gao W, Bernal R, Espinosa H. High strain rate tensile testing of silver nanowires: rate-dependent brittle-to-ductile transition. Nano Lett 2015;16(1):255–63.
[13] Peng B, Locascio M, Zapol P, Li S, Mielke SL, Schatz GC, et al. Measurements of near-ultimate strength for multiwalled carbon nanotubes and irradiation-induced crosslinking improvements. Nat Nanotechnol 2008;3(10):626–31.
[14] Xiao H, Lu Y, Wang M, Qin X, Zhao W, Luan J. Effect of gamma-irradiation on the mechanical properties of polyacrylonitrile-based carbon fiber. Carbon 2013;52:427–39.
[15] Manocha LM, Yasuda E, Tanabe Y, Kimura S. Effect of carbon fiber surface-treatment on mechanical properties of C/C composites. Carbon 1988;26(3):333–7.
[16] Johnson D. Structure-property relationships in carbon fibres. J Phys D: Appl Phys 1987;20(3):286.
[17] Papkov D, Goponenko A, Compton OC, An Z, Moravsky A, Li XZ, et al. Improved graphitic structure of continuous carbon nanofibers via graphene oxide templating. Adv Funct Mater 2013;23(46):5763–70.
[18] Matsumoto T. Mesophase pitch and its carbon fibers. Pure Appl Chem 1985;57(11):1553–62.
[19] Liu Y, Kumar S. Recent progress in fabrication, structure, and properties of carbon fibers. Polym Rev 2012;52(3):234–58.
[20] Papkov D, Beese AM, Goponenko A, Zou Y, Naraghi M, Espinosa HD, et al. Extraordinary improvement of the graphitic structure of continuous carbon nanofibers templated with double wall carbon nanotubes. ACS nano 2012;7(1):126–42.
[21] Kakida H, Tashiro K, Kobayashi M. Mechanism and kinetics of stabilization reaction of polyacrylonitrile and related copolymers I. Relationship between Isothermal Dsc thermogram and Ft/Ir spectral change of an acrylonitrile/methacrylic acid copolymer. Polym J 1996;28(1):30–4.
[22] Rafiei S, Noroozi B, Arbab S, Haghi AK. Characteristic assessment of stabilized polyacrylonitrile nanowebs for the production of activated carbon nano-sorbents. Chin J Polym Sci 2014;32(4):449–57.
[23] Wu M, Wang Q, Li K, Wu Y, Liu H. Optimization of stabilization conditions for electrospun polyacrylonitrile nanofibers. Polym Degrad Stabil 2012;97(8):1511–19.
[24] Dzenis Y., Strong and tough continuous nanofibers. Google Patents: 2013.

[25] Naraghi M, Filleter T, Moravsky A, Locascio M, Loutfy RO, Espinosa HD. A multi-scale study of high performance double-walled nanotube– polymer fibers. ACS nano 2010;4(11):6463–76.
[26] Bernal RA, Ramachandramoorthy R, Espinosa HD. Double-tilt *in situ* tem holder with multiple electrical contacts and its application in mems-based mechanical testing of nanomaterials. Ultramicroscopy 2015;156:23–8.
[27] Espinosa HD, Zhu Y, Moldovan N. Design and operation of a mems-based material testing system for nanomechanical characterization. J Microelectromech Syst 2007;16(5):1219–31.
[28] Zhu Y, Moldovan N, Espinosa HD. A microelectromechanical load sensor for *in situ* electron and X-ray microscopy tensile testing of nanostructures. Appl Phys Lett 2005;86(1):013506.
[29] Ramachandramoorthy R, Bernal R, Espinosa HD. Pushing the envelope of *in situ* transmission electron microscopy. ACS nano 2015;9(5):4675–85.
[30] Filleter T, Ryu S, Kang K, Yin J, Bernal RA, Sohn K, et al. Nucleation-controlled distributed plasticity in penta-twinned silver nanowires. Small 2012;8(19):2986–93.
[31] Zhu YT, Blumenthal WR, Taylor ST, Lowe TC, Zhou B. Analysis of size dependence of ceramic fiber and whisker strength. J Am Ceram Soc 1997;80(6):1447–52.
[32] Espinosa H, Peng B, Prorok B, Moldovan N, Auciello O, Carlisle J, et al. Fracture strength of ultrananocrystalline diamond thin films—identification of Weibull parameters. J of Appl Phys 2003;94(9):6076–84.
[33] Bergman B. On the estimation of the Weibull modulus. J Mater Sci Lett 1984;3(8):689–92.
[34] Tagawa T, Miyata T. Size effect on tensile strength of carbon fibers. Mater Sci Eng: A 1997;238(2):336–42.
[35] León, C.A.L., Carbon fibers having improved strength and modulus and an associated method and apparatus for preparing same. Google Patents: 2013.
[36] http://www.hexcel.com.
[37] http://www.toraycma.com/.
[38] Bunsell AD. The tensile and fatigue behaviour of Kevlar-49 (Prd-49) fibre. J Mater Sci 1975;10(8):1300–8.
[39] Cunniff PM, Auerbach MA, Vetter E, Sikkema DJ. In High Performance “M5” Fiber for Ballistics/Structural Composites. In: 23rd Army Science Conference; 2002. p. 1–8.